Published in final edited form as:
Cancer Res. 2011 July 15; 71(14): 4834–4845. doi:10.1158/0008-5472.CAN-11-0027.

Human Neural Stem Cell Transplantation Ameliorates Radiation-Induced Cognitive Dysfunction

Munjal M. Acharya[1], **Lori-Ann Christie**[1], **Mary L. Lan**[1], **Erich Giedzinski**[1], **John R. Fike**[2], **Susanna Rosi**[3], and **Charles L. Limoli**[1]

[1]Department of Radiation Oncology, University of California, Irvine, Irvine

[2]Brain and Spinal Injury Center, Department of Neurological Surgery, University of California, San Francisco, San Francisco, California

[3]Physical Therapy and Rehabilitation Science, University of California, San Francisco, San Francisco, California

Abstract

Cranial radiotherapy induces progressive and debilitating declines in cognition that may, in part, be caused by the depletion of neural stem cells. The potential of using stem cell replacement as a strategy to combat radiation-induced cognitive decline was addressed by irradiating athymic nude rats followed 2 days later by intrahippocampal transplantation with human neural stem cells (hNSC). Measures of cognitive performance, hNSC survival, and phenotypic fate were assessed at 1 and 4 months after irradiation. Irradiated animals engrafted with hNSCs showed significantly less decline in cognitive function than irradiated, sham-engrafted animals and acted indistinguishably from unirradiated controls. Unbiased stereology revealed that 23% and 12% of the engrafted cells survived 1 and 4 months after transplantation, respectively. Engrafted cells migrated extensively, differentiated along glial and neuronal lineages, and expressed the activity-regulated cytoskeleton-associated protein (Arc), suggesting their capability to functionally integrate into the hippocampus. These data show that hNSCs afford a promising strategy for functionally restoring cognition in irradiated animals.

Introduction

Ionizing radiation is an effective treatment for intracranial malignancies, but such therapy can induce serious adverse effects to normal tissues distal to the tumor site. Although changes involving gross tissue destruction, for example, necrosis, are not common, a significant number of patients surviving more than 6 months postradiotherapy suffer cognitive impairment that severely impacts quality of life (1, 2). The types of impairments observed encompass a broad range of cognitive domains, including disrupted memory, attention, concentration, and executive function, such as planning and multitasking (3, 4). These decrements are debilitating, persistent, and progressive and are especially problematic in pediatric patients (5, 6). Pharmacologic interventions targeted to specific central nervous system (CNS) receptors and signaling pathways have shown some promise (7–10), but, to date, none have provided the potential benefit of replacing lost or damaged cells associated

Corresponding Author: Charles L. Limoli, Department of Radiation Oncology, University of California Irvine, Medical Sciences I, Room B-149, Irvine, CA 92697. Phone: 949-824-3053; Fax: 949-824-3566; climoli@uci.edu.

Disclosure of Potential Conflicts of Interest
No potential conflicts of interest were disclosed.

with cognitive performance. This serious, currently untreated side effect is considered one of the most critical criteria for determining long-term quality of life (1).

The mechanisms underlying radiation-induced cognitive impairment are not well understood and are likely multifaceted involving microenvironmental factors such as oxidative stress and inflammation, which, in turn, can influence neural stem/progenitor cell (NSC) populations associated with cognitive function (3, 7, 8, 11–16). It is hypothesized that the relative radiation sensitivity of hippocampal NSC and their responsiveness to alterations in the microenvironment constitute critical factors in the development of learning and memory impairments (13–15, 17–19).

After irradiation, surviving NSCs respond by engaging a stress response that alters proliferation, metabolism, survival, and differentiation (12, 13), as well as the expression patterns of behaviorally activated immediate early genes such as activity-related cytoskeleton-associated protein (Arc; ref. 20). Given that the function of surviving NSCs may be adversely affected by irradiation, there is a strong rationale for pursuing transplantation-based stem cell strategies for improving cognition after cranial irradiation. Although bone marrow transplants have been used for years to reconstitute the hematopoietic system after ablative irradiation (21), the application of stem cell therapies to reduce radiation-induced normal tissue damage has thus far been restricted to the amelioration of xerostomia (22).

Recently, we used human embryonic stem cells in a rodent model to ameliorate cognitive impairment associated with ionizing irradiation (23). Although the results from that study were provocative, the use of human pluripotent embryonic stem cells has potential safety concerns such as teratoma formation (24), and is associated with complex ethical issues (25). Given these potential limitations, the identification and functional characterization of additional cell types for replacement strategies are major priorities within the stem cell community. Consequently, the focus of the present study was to establish the behavior of a lineage-restricted neural stem cell of human origin (hNSC) engrafted into an irradiated brain and to determine whether those cells could safely attenuate radiation-induced cognitive impairment. Furthermore, to address the possible mechanisms by which engrafted hNSCs might prevent cognitive decline (or improve cognition), we quantified engrafted cell survival by unbiased stereology and characterized the phenotypic fates of engrafted cells at 1 and 4 months postirradiation. Remarkably, a subpopulation of engrafted cells expressing Arc was identified, suggesting that some of the transplanted hNSCs were capable of forming new synapses within existing hippocampal circuitry. Here we describe our studies characterizing the capability of engrafted hNSCs to forestall the development of radiation-induced cognitive decline.

Materials and Methods

Animals and irradiation

All animal procedures were carried out in accordance with NIH and Institutional Animal Care and Use Committee guidelines. Host-mediated immune rejection and survival after cell engraftment are key factors that determine the success of xenograft models and stem cell-based therapies. For this reason, the constitutively immunodeficient athymic nude (ATN) rat model was used here, as in our previous study (23). A total of 65 young, male (2-month-old) ATN rats (strain 02N01 Cr:NIH-rnu; National Cancer Institute), maintained in sterile conditions, were used in this study. Animal groups included the following: nonirradiated sham surgery controls (CON; 1 month, $n = 12$; 4 month, $n = 8$); irradiated sham surgery (IRR; 1 month, $n = 9$; 4 month, $n = 12$); and irradiated with engrafted hNSCs (IRR + hNSC; 1 month, $n = 12$; 4 month, $n = 8$). An additional cohort of hNSC-engrafted animals (IRR +

hNSC; $n = 4$) was employed for our analysis of behaviorally induced Arc protein. Anesthetized rats were exposed to cranial γ-irradiation (10 Gy) by using a ^{137}Cs irradiator (J.L. Shepard and Associates Mark I) at a dose rate of 2.07 Gy/min, as previously described (20).

hNSCs and transplantation surgery

The use of human stem cells in this study was approved by UCI's Human Stem Cell Research Oversight Committee (hSCRO). The ENStem-A cell line (hNSCs; EMD Millipore) was used in this study. Each lot is routinely validated by the manufacturer for high levels of expression of nestin and Sox2, and low-level expression of Oct-4, along with the ability to differentiate into multiple neuronal phenotypes and to maintain a normal karyotype after multiple passages. In our laboratory, hNSCs maintained as monolayers in neural expansion media (Millipore) displayed abundant expression of Sox2 and nestin and retained their ability to differentiate, as described previously (13). For the present studies, hNSCs were used at passages 4 to 8. Prior to engraftment, hNSCs were labeled with 5-bromo-2′-deoxyuridine (BrdUrd; Sigma-Aldrich) by supplementing the hNSC culture media with 4 μmol/L BrdUrd for 3 days. BrdUrd incorporation was detected using immunocytochemistry and visualized using a mouse anti-BrdUrd antibody (1:200 dilution; Invitrogen), as described previously (23). The *in vitro* BrdUrd index for all transplantation studies was 90 ± 2.2% (mean ± SEM, $n = 12$).

Cultures of hNSCs, prepared as described, were then used for the subsequent studies detailed in the schematic illustration of our research design (Fig. 1J). Irradiated rats received bilateral, intrahippocampal engraftment of BrdUrd-labeled hNSCs 2 days after cranial irradiation (IRR + hNSC). A total of 1.0×10^5 live hNSCs were injected in 1 μL of the cell suspension by using a 33-gauge microsyringe at an injection rate of 0.25 μL/min. Both hippocampi received 4 distinct injections (total 4.0×10^5 live hNSCs per hemisphere) by using precise stereotaxic coordinates (23). Control and irradiated rats receiving sterile vehicle (neural expansion media) at the same stereotaxic coordinates served as sham surgery groups.

Assessment of cognition

Groups of rats were tested on a novel place recognition (NPR) task at 1 or 4 months postengraftment. The NPR task uses spontaneous exploration as a means of assessing spatial recognition memory, which has been shown previously to rely on intact hippocampal function (26, 27). A standard protocol (23) was followed employing Ethovision XT software (v5.0; Noldus Information Technology, Inc.) for automated tracking and exploration detection, with exploration defined as the animal's head being directed toward and located within a 2-cm radius of the stimulus.

Immunohistochemistry, stereology, and confocal microscopy

At 1 and 4 months postengraftment (after cognitive testing), animals were euthanized by intracardiac perfusion with 4% paraformaldehyde. Processing of all tissue sections followed standard procedures (23). For studies of Arc protein, a separate cohort of animals was subjected to the NPR task, decapitated exactly 30 minutes later, and their brains were frozen in isopentane and sectioned coronally as described previously (20).

For stereologic quantification, every 10th section through the entire hippocampus was processed for BrdUrd immunostaining (mouse anti-BrdUrd, clone AH4H7-1/131-14871, 1:200; Millipore). Color was developed using the avidin-biotin-complex method and enhanced diaminobenzidine substrate (Vector Labs), and all sections were counterstained with hematoxylin. Stereologic enumeration was conducted using an Olympus BX60

microscope equipped with an MBF CX9000 color digital camera, 100 × (oil-immersion, 1.30NA) objective lens, 3-axis motorized stage and StereoInvestigator software (MBF Biosciences, v9). The yield of surviving hNSCs was quantified by counting BrdUrd-positive nuclei using the optical fractionator probe, and systematic random sampling of the BrdUrd-stained section was carried out according to unbiased stereology principles. Sampling parameters (grid and counting frame size) were empirically determined to achieve low coefficients of error (<0.031 ± 0.002; $n = 8$) for hippocampus.

For dual immunofluorescence analyses, we utilized anti-BrdUrd (purified rat, 1:200; Millipore), anti-neuron–specific nuclear antigen (anti-NeuN; mouse, 1:250; Millipore), anti-glial fibrillary acidic protein (anti-GFAP; mouse, 1:500; Invitrogen), antinuclei (human specific antinuclei, HuNu, mouse clone 235-1, 1:150; Millipore), nestin (mouse, 1:200; Millipore), Ki67 (rabbit, 1:150; Millipore), S100ß protein (S100, 1:200, rabbit; Millipore), and ß-III-tubulin (Tuj1, rabbit, 1:200; Covance) antibodies and polyclonal rabbit anti-Arc antibody (1:500; a kind gift from Dr. P.F. Worley, Johns Hopkins University, Baltimore, MD). The secondary antibodies included biotinylated antimouse, antirat, and antirabbit IgG (goat and donkey, 1:200; Vector Labs), goat antimouse, antirat, and antirabbit IgG conjugated to Alexa Fluor (488 and 594, 1:200; Invitrogen). For the quantification of hNSC differentiation, representative hippocampal sections from 4 to 6 distinct transplant sites derived from 4 engrafted animals were subjected to dual immunofluorescence staining. Sections were immunostained for BrdUrd in conjunction with neuronal (NeuN and Tuj1), astrocytic (GFAP and S100), cell-cycle, and multipotent markers (Ki67 and nestin) using standard protocols and analyzed using laser scanning confocal microscopy (Nikon Eclipse TE2000-U, EZ–C1 inter-face), as described previously (23). Analysis of Arc expression was accomplished using a Zeiss Axio Imager Z1 microscope equipped with a motorized Z-drive for transmitted light and epifluorescence (20). Analyses of Z-sections were carried out using 1-μm stack intervals, and orthogonal image reconstruction was done using Nikon Elements AR software (v3.10).

Statistical analyses

Exploration ratio, or the proportion of total time spent exploring the novel spatial location ($t_{novel}/t_{novel} + t_{familiar}$), was used as the main dependent measure for statistical analyses. We analyzed the behavior of the animals during minute 1 of the 5-minute and 24-hour test phases; previous research has shown that preference for the novel place diminishes after the first minute, as the spatial locations become equally familiar to the animals (26). To establish baseline exploratory behavior, we also analyzed exploration of the stimuli during the initial familiarization phase.

Analyses of cognitive data were carried out using PASW Statistics version 17.0 (SPSS Inc.). Analyses for the 1- and 4-month posttransplantation times were conducted separately. Group sample sizes for the statistical analyses were as follows: CON (1 month, $n = 12$; 4 month, $n = 8$); IRR (1 month, $n = 9$; 4-month, $n = 12$); and IRR + hNSC (1 month, $n = 8$; 4 month, $n = 8$). In all statistical tests were 2-tailed, and values of $P < 0.05$ were considered statistically significant.

Exploration ratio data were analyzed using univariate ANOVAs for the 5-minute and 24-hour test phases. In all cases, we confirmed that the data were normally distributed using the Kolmogorov–Smirnov test, and that the error variances did not differ between groups by using Levene's test of equality of error variances. When a statistically significant overall group effect was found, multiple comparisons were made using Fisher's protected least significant difference (FPLSD) post hoc tests to compare the individual groups. Additional analyses of recognition memory were conducted using 1-sample t tests to determine whether the mean proportion of time spent exploring the novel spatial location for each group

differed significantly from chance (i.e., 0.5). For stereologic analyses, 2-tailed Student's *t* tests were used and a value of $P \leq 0.05$ was considered statistically significant.

Results

Characterization of hNSCs

The EnStem-A hNSC line used in this study was characterized for the expression of multipotent markers *in vitro*. hNSCs maintained as monolayers displayed abundant expression of Sox2 and nestin (13). To trace the presence of grafted cells in host tissue, hNSCs were labeled with BrdUrd *in vitro*. Immunostaining against human-specific nuclear antigen (HuNu) was used to cross-validate the presence of $BrdUrd^+$ human cells in brain sections of rats engrafted with hNSCs (Fig. 1). Dual labeling of BrdUrd and HuNu was confirmed *in vitro* (Fig. 1A–C), and the correspondence between these 2 markers *in vivo* at 1 month (Fig. 1D–F) and 4 months (Fig. 1G–I) postgrafting indicated that grafted cells did not undergo extensive proliferation. A schematic illustration of our research design is shown in Figure 1J.

hNSC engraftment restores cognition

One month postengraftment—One month after engraftment, rats were habituated and tested on the NPR task. For the 5-minute test, group means and 95% CIs were as follows: IRR (mean = 0.159, 95% CI = −0.097 to 0.415); CON (mean = 0.822, 95% CI = 0.653–0.990); and IRR + hNSC (mean = 0.888, 95% CI = 0.775–0.999). An overall significant group difference was found for exploration ratio following the short, 5-minute retention interval [Fig. 2A; $F(2, 26) = 21.58$; $P < 0.001$]. IRR animals showed significantly decreased preference for the novel spatial location compared with both CON ($P < 0.0001$) and IRR + hNSC ($P < 0.0001$) animals. In contrast, IRR + hNSC animals showed similar preference for the novel spatial location as nonirradiated controls ($P = 0.587$). Furthermore, 1-sample *t* tests comparing group exploration ratios to chance (i.e., 0.5) revealed that like controls ($P = 0.001$), IRR + hNSC animals explored the novel spatial location significantly more than expected by chance ($P < 0.001$), whereas IRR animals explored the novel spatial location significantly less than expected by chance ($P = 0.015$).

Following the 24-hour delay=(Fig. 2B), IRR animals (mean = 0.288, 95% CI = 0.0068–0.5824) again showed decreased preference for the novel place compared with CON (mean = 0.583, 95% CI 0.326–0.841), and IRR + hNSC animals (mean = 0.495, 95% CI = 0.861), and IRR + hNSC animals (mean = 0.495, 95% CI = 0.129–0.861), although the overall group difference was not significant [$F(2, 26) = 0.166$, $P = 0.848$]. One-sample *t* tests showed that none of the groups explored the novel spatial location significantly more or less than expected by chance following the 24-hour delay (all *P*s > 0.14). Similar trends were observed for total time spent exploring the novel and familiar spatial locations across the entire 3-minute test sessions of the 5-minute and 24-hour test phases (Fig. 2C and D, respectively). An overall group difference was found when exploration time was assessed during the familiarization phase, when the 2 spatial positions were equally unfamiliar to the animals [Fig. 2E; $F(2, 26) = 11.354$; $P < 0.001$]; IRR animals (mean = 6.173, 95% CI = 11.666–10.680) spent less time exploring overall than both CON (mean = 12.902, 95% CI = 8.607–17.197, $P = 0.032$) and IRR + hNSC animals (mean = 21.747, 95% CI = 15.416–28.078, $P < = 0.001$).

Four months postengraftment—In a separate experiment, rats were habituated and tested on the NPR task 4 months postengraftment. For the 5-minute test, group means and 95% CIs were as follows: IRR (mean = 0.394, 95% CI = 0.133–0.655); CON (mean = 0.781, 95% CI = 0.517–1.045); and IRR + hNSC (mean = 0.691, 95% CI = 0.487–0.895). An

overall significant group difference was found for exploration ratio following the short, 5-minute retention interval [Fig. 3A; $F(2, 25) = 3.512$, $P = 0.045$]. IRR animals showed significantly decreased preference for the novel spatial location compared with control animals ($P = 0.021$), whereas IRR + hNSC animals showed similar preference for the novel spatial location as controls ($P = 0.606$). One-sample *t* tests revealed that CON animals explored the novel spatial location significantly more than expected by chance (Fig. 3A; $P = 0.04$). Similarly, IRR + hNSC animals tended explore the novel place more than chance ($P = 0.062$) whereas IRR animals did not ($P = 0.391$), suggesting = that they did not remember the familiar spatial location following the 5-minute delay interval.

A significant overall group effect was found on the 24-hour test [Fig. 3B, $F(2, 25) = 5.029$; $P = 0.014$], and post hoc tests showed that IRR animals (mean = 0.134, 95% CI = −0.072 to 0.340) were impaired compared with CON (mean = 0.628, 95% CI = 0.339–0.916, $P = 0.004$) whereas IRR + hNSC animals (mean = 0.363, 95% CI = 0.065–0.660) did not differ from CON ($P = 0.153$). Furthermore, 1-sample *t* tests showed that IRR animals explored the novel spatial location significantly less than expected by chance ($P = 0.002$). Similar trends were observed in plots of total time spent exploring the novel and familiar spatial locations across the 3-minute test sessions for both the 5-minute and 24-hour test phases (Fig. 3C and D, respectively). Group differences were also found when exploration time was assessed during the initial familiarization phase [Fig. 3E; $F(2, 25) = 4.67$, $P = 0.044$]; IRR animals (mean = 9.193, 95% CI = 5.946–12.439) spent less time exploring the equally familiar spatial positions than both CON (mean = 15.119, 95% CI = 10.087–20.151, $P = 0.037$) and IRR + hNSC animals (mean = 15.257, 95% CI = 9.512–21.0, $P = 0.033$).

hNSCs survive and migrate throughout the host hippocampus at both 1- and 4-month time points

Analysis of brain sections from the 1-month postengraftment group using BrdUrd immunostaining revealed the presence of engrafted cells in the host hippocampus (Fig. 4A–D). Engrafted cells migrated extensively from the injection site throughout the hippocampus. Further analyses of BrdUrd-stained sections showed grafted cells in the dentate gyrus (DG), dentate hilus (DH), and CA3 and CA1 subfields (Fig 4A–D) and partly in corpus callosum (CC; Fig. 4A). Similar incorporation and migration patterns of engrafted cells were observed in the 4-month postengraftment group. In addition, engrafted cells were found to target the dentate subgranular zone (SGZ), the neurogenic niche of the hippocampus, at both the 1- and 4-month postengraftment time points, corroborating our previous findings with hNSCs (23). Furthermore, stereologic quantification of 1- and 4-month postgrafting tissues revealed grafted cell survival levels of 23.2% and 12.5%, respectively [Fig. 4E; $t(6) = 4.662$, $P = 0.004$, 95% CI = 5.105–16.38]. These relative yields translated= to an average of approximately 123,000 and 49,000 new cells added to each hemisphere at 1 and 4 months postengraftment, respectively.

Phenotypic fate of engrafted hNSCs

To ascertain the fate of engrafted cells, glial, neuronal, and functional markers were assessed in conjunction with BrdUrd labeling 1 and 4 months after grafting. $BrdUrd^+/NeuN^+$ engrafted cells were observed throughout the hippocampus at both times (Fig. 5A and C). Notably, mature neuronal morphology, as shown in orthogonal reconstructions (Fig. 5a and c), was predominantly located in the SGZ and CA1 subfields of the hippocampus. Astrocytic differentiation ($BrdUrd^+/GFAP^+$) was also apparent at both postengraftment times (Fig. 5B, b and D, d). Although $BrdUrd^+/GFAP^+$ engrafted cells were located throughout the hippocampus, astrocytic differentiation was most predominant in the CC.

To investigate the impact of the irradiated tissue bed on the phenotypic fate of engrafted hNSCs, we quantified the expression of neuronal and astrocytic markers (Fig. 6B–D). To determine the cell-cycle and multipotent status of engrafted cells, nestin and Ki67 staining were assessed (Fig. 6A and B). Quantification of engrafted cells revealed 12% mature ($NeuN^+$) and 9% immature ($Tuj1^+$) neuronal differentiation at 1 month postengraftment (Fig. 6B). Astroglial differentiation at this time showed equal distributions (~16% each) of mature ($S100ß^+$) and immature ($GFAP^+$) astrocytic cell types (Fig. 6B). Thus, 1 month after transplantation, 21% of engrafted cells differentiated into neurons and 32% into astrocytes (Fig. 6C). At 4 months postengraftment, 10% of the transplanted hNSCs differentiated into mature ($NeuN^+$) and 5% into immature neurons ($Tuj1^+$; Fig. 6B). At this same time, astrocytic differentiation was 19% mature ($S100ß^+$) and 27% immature ($GFAP^+$; Fig. 6B), yielding total cell fates of 15% neuronal and 46% astrocytic (Fig 6C). In addition, 1% and 4% of the engrafted ($BrdUrd^+$) cells remained positive for nestin whereas 4% and 2% stained positive for Ki67 at 1 and 4 months postengraftment, respectively (Fig. 6B). Extrapolating these yields of differentiated cell types based on stereologic estimates, transplantation of hNSC resulted in the addition of approximately 26,000 neurons and 39,000 astrocytes at 1 month postengraftment whereas approximately 7,500 neurons and 22,700 astrocytes were added at 4 months postengraftment (Fig. 6D) into each hemisphere of irradiated animals.

Engrafted hNSCs express behaviorally induced Arc

Our past (23) and current works show that hippocampal engrafted pluripotent or multipotent stem cells develop along glial and neuronal lineages. The fact that a subset of engrafted cells adopted mature neuronal morphology within the CA1 subfield suggested that these cells might have integrated into the hippocampal circuitry. To test this idea, a cohort of animals euthanized 30 minutes after testing on the NPR task was analyzed for the presence of Arc-positive engrafted cells. A representative sample of hNSCs (~150 engrafted cells/animal) was assessed for the coexpression of BrdUrd and the behaviorally-induced immediate early gene product, Arc (Fig. 7). Approximately 70 of these engrafted cells (i.e., 11% ± 4%, mean ± SEM, $n = 4$) were colabeled ($BrdUrd^+/Arc^+$) and were predominantly located in the CA1 area (Fig. 7A). A small fraction of the $BrdUrd^+/Arc^+$ cells also colabeled with NeuN (Fig. 7B–M).

Discussion

Here we report that intrahippocampal engraftment of hNSCs prevented the development of radiation-induced cognitive impairment, showing that engraftment of multipotent stem cells can protect the brain from a serious side effect of cranial irradiation. Following irradiation and engraftment, hNSCs survived, migrated extensively throughout the hippocampus, and expressed neuronal and astrocytic markers (Figs. 4–6). Engrafted cell survival quantified by unbiased stereology revealed that 23% and 12% of the transplanted cells survived at 1 and 4 months, respectively (Fig. 4). Quantification of phenotypic fate of the engrafted hNSCs at these times revealed the addition of both immature and mature neurons and astroglial cell types in the irradiated hippocampus (Fig. 6). Thus, as few as approximately 100,000 surviving cells (15% neuronal, 45% astroglial) in the irradiated brain were sufficient to prevent the cognitive deficits observed in irradiated rats receiving no engraftment. Although the mechanism(s) of stem cell–based cognitive rescue has not been elucidated, it is likely that some combination of functional replacement and/or trophic support is playing a role. The identification of Arc-positive engrafted cells suggests that the transplanted hNSCs can functionally integrate into the hippocampal circuitry (Fig. 7), which points to a possible mechanism for stem cell–based effects on cognition after cranial irradiation.

The assessment of cognitive performance was accomplished using an NPR task. Successful performance of this task depends on intact hippocampal function (26, 27). The present findings corroborate prior behavioral findings and suggest that radiation-induced alterations in cognition are caused, in part, by injury to the hippocampus (28, 29). Irradiated animals that received vehicle injections exhibited significantly impaired NPR, showing that short- (5 minutes) and long-term (24 hours) memory for a specific spatial arrangement of the objects was impaired by exposure to 10 Gy head-only irradiation (Fig. 2). In contrast, irradiated animals transplanted with hNSCs (IRR + hNSC) did not display impaired spatial memory and their performance was comparable with that of unirradiated controls, showing the ability of engrafted cells to prevent radiation-induced cognitive dysfunction.

The behaviorally induced immediate early gene *Arc*, and its protein product, is induced in the hippocampus by spatial exploration (30–32). Arc is rapidly activated by robust patterned synaptic activity related to learning and memory behavior (33), and altering Arc expression impairs spatial learning and long-term potentiation (34). Therefore, Arc expression has been used extensively to map neuronal networks that underlie information processing and plasticity (30, 31). Our data showing the presence of $BrdUrd^+/Arc^+/NeuN^+$ engrafted cells suggest that some of the transplanted cells integrated into existing neuronal circuits (Fig. 7), although the full extent of such integration and its functional significance remains to be determined. A recent report found a gradual, time-dependent increase in Arc expression in newly born DG cells that eventually differentiated into mature neurons and incorporated into the hippocampal circuitry (35). Stereologic estimates derived from the 1-month postgrafting time showed an average survival of 123,000 engrafted cells per hippocampus. Extrapolating this number yields approximately 13,500 cells expressing Arc in each hippocampus or approximately 27,000 per brain. Whether these engrafted cells prevent cognitive decline or actually improve cognition is uncertain at this time, but the recent finding of super-connected “hub” cells in the brain (36, 37) suggests the intriguing possibility that engrafted stem cells may be preferentially recruited as such cells to foster and preserve the functional connectivity of the CNS (37).

Functional integration of engrafted hNSCs within the hippocampus may not be necessary or sufficient for cognitive rescue. Restoration of damaged synaptic circuits may also require the presence of glial cells to support preexisting neurons. Grafted glial cells may serve to repair or improve the function of existing cells either directly, or indirectly, by mediating the remodeling of the irradiated microenvironment (38, 39). We found 32% and 46% astroglial differentiation of engrafted hNSCs at 1- and 4-month postengraftment group, respectively (Fig. 6C). This resulted in the addition of 78,000 and 45,000 astrocytes (Fig. 6D) in the irradiated hippocampus. Significant past work using various injury and disease models suggests that engrafted cells secrete a range of beneficial growth factors, such as glial cell line–derived neurotrophic factor (40, 41), and brain-derived neurotrophic factor (42). The positive influence that engrafted cells have on cognition is noteworthy given the duration of the postirradiation intervals and the multifaceted nature of learning and memory. Future studies will determine whether engrafted cells exert longer-lasting changes in synaptic plasticity, if that effect is dependent on integration of cells into the hippocampal circuitry and/or if it is facilitated through trophic support.

The hNSCs used here were multipotent based on marker expression *in vitro* (13), and the BrdUrd labeling indices of the cells was approximately 90%. Noteworthy too was the absence of any overt adverse cognitive sequelae (e.g., ataxia) in the cohort of animals receiving hNSC grafting, suggesting that intracranial teratogenesis and/or hyperproliferation was not problematic over the duration of this study. This was supported by the small fraction of transplanted cells that remained multipotent ($nestin^+$) and/or retained their capacity to proliferate ($Ki67^+$; Fig. 6A and B). Analysis of brain sections revealed that engrafted cells

migrated extensively throughout the hippocampus (Fig. 4). Engrafted cells near the SGZ or at other hippocampal sites such as the CA1 showed characteristic signs of differentiation, as mature neurons and glia developed morphology that is distinct to those lineages (Figs. 5 and 6).

Our current studies have now clearly shown the benefits of engrafted stem cells for reversing cognitive impairments following cranial irradiation. Moving these promising results into the clinic for the treatment of radiation-induced cognitive dysfunction along with other degenerative conditions will require careful consideration of many potential limitations including immunorejection and tumorigenesis (24). Use of patient-derived induced pluripotent stem cells may one day alleviate certain practical concerns (43), but considerable effort is still required to further define mechanisms and optimal treatment parameters. These efforts will help determine the timeline and feasibility of using similar stem cell–based therapies as safe and effective options in humans. The capability to minimize the adverse cognitive sequelae associated with cranial radiotherapy is encouraging and points to the promise of using stem cell–based strategies for minimizing normal tissue damage.

Acknowledgments

We are grateful to Drs. Aileen J. Anderson and Brian J. Cummings for generously providing access to stereology equipment.

Grant Support

This work was supported by California Institute for Regenerative Medicine (CIRM) Seed grant RS1-00413 (C.L. Limoli), NIH NINDS grant R01 NS074388 (C.L. Limoli), Office of Science (BER) U.S. Department of Energy grant no. DE-FG02-09ER64798 (C.L. Limoli), and CIRM training grant TG2-01152 (M.M. Acharya).

References

1. Abayomi OK. Pathogenesis of irradiation-induced cognitive dysfunction. Acta Oncol. 1996; 35:659–63. [PubMed: 8938210]
2. Anderson VA, Godber T, Smibert E, Weiskop S, Ekert H. Cognitive and academic outcome following cranial irradiation and chemotherapy in children: a longitudinal study. Br J Cancer. 2000; 82:255–62. [PubMed: 10646874]
3. Raber J. Unintended effects of cranial irradiation on cognitive function. Toxicol Pathol. 2010; 38:198–202. [PubMed: 19880825]
4. Meyers CA, Geara F, Wong PF, Morrison WH. Neurocognitive effects of therapeutic irradiation for base of skull tumors. Int J Radiat Oncol Biol Phys. 2000; 46:51–5. [PubMed: 10656372]
5. Roman DD, Sperduto PW. Neuropsychological effects of cranial radiation: current knowledge and future directions. Int J Radiat Oncol Biol Phys. 1995; 31:983–98. [PubMed: 7860415]
6. Moore BD III, Copeland DR, Ried H, Levy B. Neurophysiological basis of cognitive deficits in long-term survivors of childhood cancer. Arch Neurol. 1992; 49:809–17. [PubMed: 1524513]
7. Conner KR, Payne VS, Forbes ME, Robbins ME, Riddle DR. Effects of the AT1 receptor antagonist L-158,809 on microglia and neurogenesis after fractionated whole-brain irradiation. Radiat Res. 2010; 173:49–61. [PubMed: 20041759]
8. Ramanan S, Kooshki M, Zhao W, Hsu FC, Riddle DR, Robbins ME. The PPARalpha agonist fenofibrate preserves hippocampal neurogenesis and inhibits microglial activation after whole-brain irradiation. Int J Radiat Oncol Biol Phys. 2009; 75:870–7. [PubMed: 19801103]
9. Zhao W, Payne V, Tommasi E, Diz DI, Hsu FC, Robbins ME. Administration of the peroxisomal proliferator-activated receptor gamma agonist pioglitazone during fractionated brain irradiation prevents radiation-induced cognitive impairment. Int J Radiat Oncol Biol Phys. 2007; 67:6–9. [PubMed: 17189061]

10. Yazlovitskaya EM, Edwards E, Thotala D, Fu A, Osusky KL, Whetsell WO Jr, et al. Lithium treatment prevents neurocognitive deficit resulting from cranial irradiation. Cancer Res. 2006; 66:11179–86. [PubMed: 17145862]
11. Mizumatsu S, Monje M, Morhardt D, Rola R, Palmer T, Fike J. Extreme sensitivity of adult neurogenesis to low doses of X-irradiation. Cancer Res. 2003; 63:4021–7. [PubMed: 12874001]
12. Limoli C, Giedzinski E, Rola R, Otsuka S, Palmer T, Fike J. Radiation response of neural precursor cells: Linking cellular sensitivity to cell cycle checkpoints, apoptosis and oxidative stress. Radiat Res. 2004; 161:17–27. [PubMed: 14680400]
13. Acharya MM, Lan ML, Kan VH, Patel NH, Giedzinski E, Tseng BP, et al. Consequences of ionizing radiation-induced damage in human neural stem cells. Free Radic Biol Med. 2010; 49:1846–55. [PubMed: 20826207]
14. Clelland CD, Choi M, Romberg C, Clemenson GD Jr, Fragniere A, Tyers P, et al. A functional role for adult hippocampal neurogenesis in spatial pattern separation. Science. 2009; 325:210–3. [PubMed: 19590004]
15. Fike JR, Rosi S, Limoli CL. Neural precursor cells and central nervous system radiation sensitivity. Semin Radiat Oncol. 2009; 19:122–32. [PubMed: 19249650]
16. Monje ML, Toda H, Palmer TD. Inflammatory blockade restores adult hippocampal neurogenesis. Science. 2003; 302:1760–5. [PubMed: 14615545]
17. Fishman K, Baure J, Zou Y, Huang TT, Andres-Mach M, Rola R, et al. Radiation-induced reductions in neurogenesis are ameliorated in mice deficient in CuZnSOD or MnSOD. Free Radic Biol Med. 2009; 47:1459–67. [PubMed: 19703553]
18. Limoli CL, Rola R, Giedzinski E, Mantha S, Huang TT, Fike JR. Cell-density-dependent regulation of neural precursor cell function. Proc Natl Acad Sci U S A. 2004; 101:16052–7. [PubMed: 15522966]
19. Rola R, Zou Y, Huang TT, Fishman K, Baure J, Rosi S, et al. Lack of extracellular superoxide dismutase (EC-SOD) in the microenvironment impacts radiation-induced changes in neurogenesis. Free Radic Biol Med. 2007; 42:1133–45. discussion 1–2. [PubMed: 17382195]
20. Rosi S, Andres-Mach M, Fishman KM, Levy W, Ferguson RA, Fike JR. Cranial irradiation alters the behaviorally induced immediate-early gene arc (activity-regulated cytoskeleton-associated protein). Cancer Res. 2008; 68:9763–70. [PubMed: 19047155]
21. Greenberger JS, Epperly M. Bone marrow-derived stem cells and radiation response. Semin Radiat Oncol. 2009; 19:133–9. [PubMed: 19249651]
22. Lombaert IM, Brunsting JF, Wierenga PK, Faber H, Stokman MA, Kok T, et al. Rescue of salivary gland function after stem cell transplantation in irradiated glands. PLoS One. 2008; 3:e2063. [PubMed: 18446241]
23. Acharya MM, Christie LA, Lan ML, Donovan PJ, Cotman CW, Fike JR, et al. Rescue of radiation-induced cognitive impairment through cranial transplantation of human embryonic stem cells. Proc Natl Acad Sci U S A. 2009; 106:19150–5. [PubMed: 19901336]
24. Knoepfler PS. Deconstructing stem cell tumorigenicity: a roadmap to safe regenerative medicine. Stem Cells. 2009; 27:1050–6. [PubMed: 19415771]
25. Daley GQ, Ahrlund Richter L, Auerbach JM, Benvenisty N, Charo RA, Chen G, et al. Ethics. The ISSCR guidelines for human embryonic stem cell research. Science. 2007; 315:603–4.
26. Mumby DG, Gaskin S, Glenn MJ, Schramek TE, Lehmann H. Hippocampal damage and exploratory preferences in rats: memory for objects, places, and contexts. Learn Mem. 2002; 9:49–57. [PubMed: 11992015]
27. Save E, Buhot MC, Foreman N, Thinus-Blanc C. Exploratory activity and response to a spatial change in rats with hippocampal or posterior parietal cortical lesions. Behav Brain Res. 1992; 47:113–27. [PubMed: 1590944]
28. Raber J, Rola R, LeFevour A, Morhardt D, Curley J, Mizumatsu S, et al. Radiation-induced cognitive impairments are associated with changes in hippocampal neurogenesis. Radiat Res. 2004; 162:39–47. [PubMed: 15222778]
29. Rola R, Raber J, Rizk A, Otsuka S, VandenBerg SR, Morhardt DR, et al. Radiation-induced impairment of hippocampal neurogenesis is associated with cognitive deficits in young mice. Exp Neurol. 2004; 188:316–30. [PubMed: 15246832]

30. Ramírez-Amaya V, Vazdarjanova A, Mikhael D, Rosi S, Worley PF, Barnes CA. Spatial exploration-induced Arc mRNA and protein expression: evidence for selective, network-specific reactivation. J Neurosci. 2005; 25:1761–8. [PubMed: 15716412]

31. Rosi S, Ramirez-Amaya V, Vazdarjanova A, Worley PF, Barnes CA, Wenk GL. Neuroinflammation alters the hippocampal pattern of behaviorally induced Arc expression. J Neurosci. 2005; 25:723–31. [PubMed: 15659610]

32. Rosi S, Ramirez-Amaya V, Vazdarjanova A, Esparza EE, Larkin PB, Fike JR, et al. Accuracy of hippocampal network activity is disrupted by neuroinflammation: rescue by memantine. Brain. 2009; 132:2464–77. [PubMed: 19531533]

33. Guzowski JF. Insights into immediate-early gene function in hippocampal memory consolidation using antisense oligonucleotide and fluorescent imaging approaches. Hippocampus. 2002; 12:86–104. [PubMed: 11918292]

34. Guzowski JF, Layford GL, Stevenson GD, Houston FP, McGaugh JL, Worley PF, et al. Inhibition of activity-dependent arc protein expression in the rat hippocampus impairs the maintenance of long-term potentiation and the consolidation of long-term memory. J Neurosci. 2000; 20:3993–4001. [PubMed: 10818134]

35. Kuipers SD, Tiron A, Soule J, Messaoudi E, Trentani A, Bramham CR. Selective survival and maturation of adult-born dentate granule cells expressing the immediate early gene Arc/Arg3.1. PLoS One. 2009; 4:e4885. [PubMed: 19290048]

36. Bonifazi P, Goldin M, Picardo MA, Jorquera I, Cattani A, Bianconi G, et al. GABAergic hub neurons orchestrate synchrony in developing hippocampal networks. Science. 2009; 326:1419–24. [PubMed: 19965761]

37. Case M, Soltesz I. Discreet charm of the GABAergic bourgeoisie: superconnected cells conduct developmental symphonies. Neuron. 2009; 64:780–2. [PubMed: 20064385]

38. Chiang CS, Hong JH, Stalder A, Sun JR, Withers HR, McBride WH. Delayed molecular responses to brain irradiation. Int J Radiat Biol. 1997; 72:45–53. [PubMed: 9246193]

39. Ramanan S, Zhao W, Riddle DR, Robbins ME. Role of PPARs in radiation-induced brain injury. PPAR Res. 2010; 2010:234975. [PubMed: 19789638]

40. Chen BGX, Yang CX, Tan SK, Sun ZL, Yan NH, Pang YG, et al. Neuroprotective effect of grafting GDNF gene-modified neural stem cells on cerebral ischemia in rats. Brain Res. 2009; 1284:1. [PubMed: 19520066]

41. Kameda MST, Takahashi K, Muraoka K, Kurozumi K, Yasuhara T, Maruo T, et al. Adult neural stem and progenitor cells modified to secrete GDNF can protect, migrate and integrate after intracerebral transplantation in rats with transient forebrain ischemia. Eur J Neurosci. 2007; 26:1462–78. [PubMed: 17880388]

42. Blurton-Jones M, Kitazawa M, Martinez-Coria H, Castello NA, Muller FJ, Loring JF, et al. Neural stem cells improve cognition via BDNF in a transgenic model of Alzheimer disease. Proc Natl Acad Sci USA. 2009; 106:13594–9. [PubMed: 19633196]

43. Takahashi K, Yamanaka S. Induction of pluripotent stem cells from mouse embryonic and adult fibroblast cultures by defined factors. Cell. 2006; 126:663–76. [PubMed: 16904174]

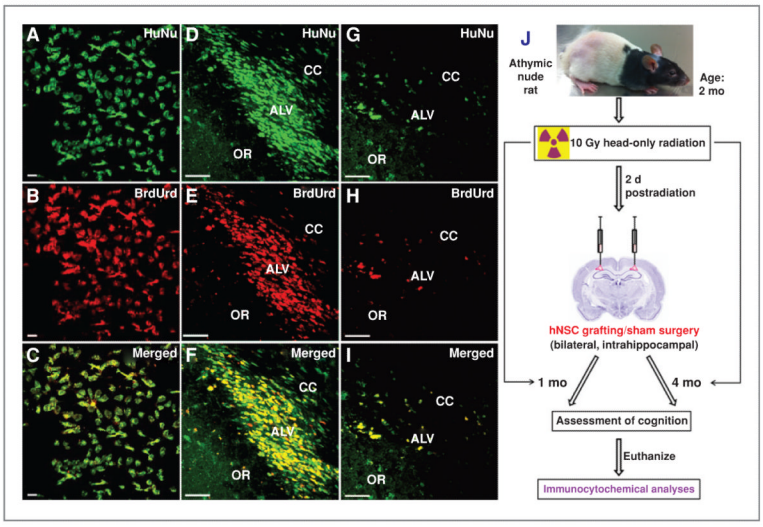

Figure 1.

In vitro and *in vivo* colabeling of HuNu (green) and BrdUrd (red). Dual labeling of HuNu with BrdUrd *in vitro* (A–C) and *in vivo* at 1 month (D–F) and 4 month (G–I) postgrafting in host hippocampus. ALV, alves of hippocampus; OR, oriens of hippocampus. Schematic illustration of transplantation studies (J). Two-month-old athymic nude rats receiving 10 Gy head-only irradiation were engrafted with hNSCs 2 days later. At 1 or 4 months following surgery, animals were subjected to cognitive testing, using the hippocampal dependent NPR task and then euthanized for engrafted cell survival and differentiation analyses. Control and irradiated animals receiving sterile vehicle served as sham surgery groups. Scale bars: A–C, 10 μm; D–I, 50 μm.

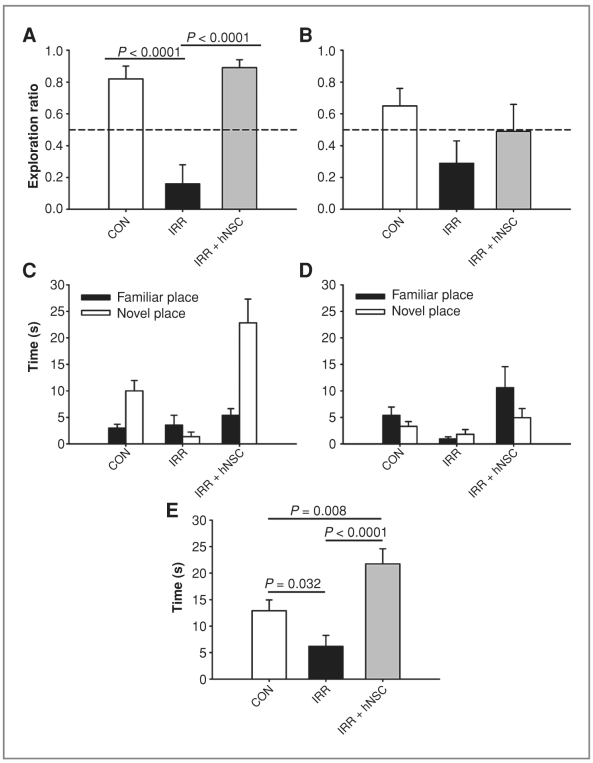

Figure 2.

Human neural stem cell engraftment improves radiation-induced impairments in NPR assessed 1 month postimplantation. A and B, exploration ratios (i.e., $t_{novel}/t_{novel} + t_{familiar}$) for the first minute of the 5-minute and 24-hour test sessions, respectively. C and D, plots of total exploration time over the entire 3-minute test session for the 5-minute and 24-hour test sessions, respectively. E, time spent exploring both objects during the initial familiarization phase. Data are presented as means + SEM, and the dashed lines (in A and B) indicate chance performance (i.e., 0.5). *P* values are derived from FPLSD post hoc comparisons.

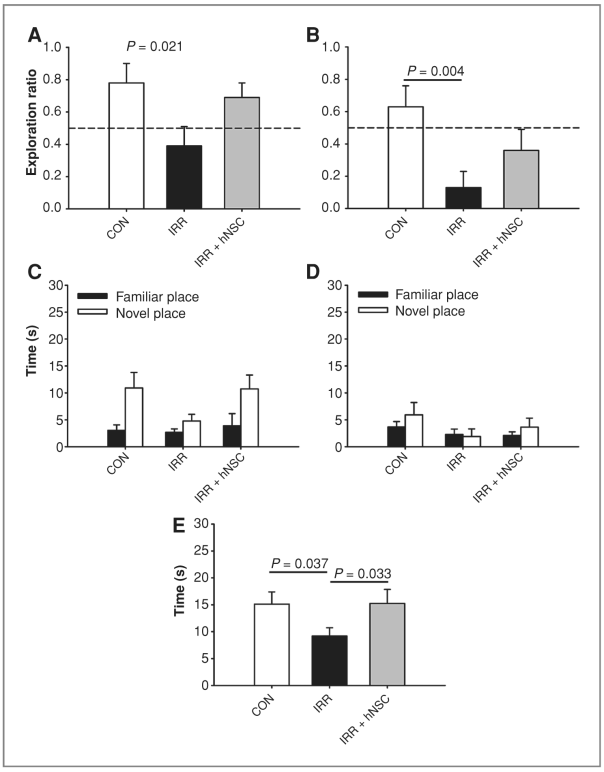

Figure 3.

Human neural stem cell engraftment improves radiation-induced impairments in NPR assessed 4 months postimplantation. A and B, exploration ratios (i.e., $t_{novel}/t_{novel} + t_{familiar}$) for the first minute of the 5-minute and 24-hour test sessions, respectively. C and D, plots of total exploration time over the entire 3-minute test sessions for the 5-minute and 24-hour test sessions, respectively. E, time spent exploring both objects during the initial familiarization phase. Data are presented as means + SEM, and the dashed lines (in A and B) indicate chance performance. *P* values are derived from FPLSD post hoc comparisons.

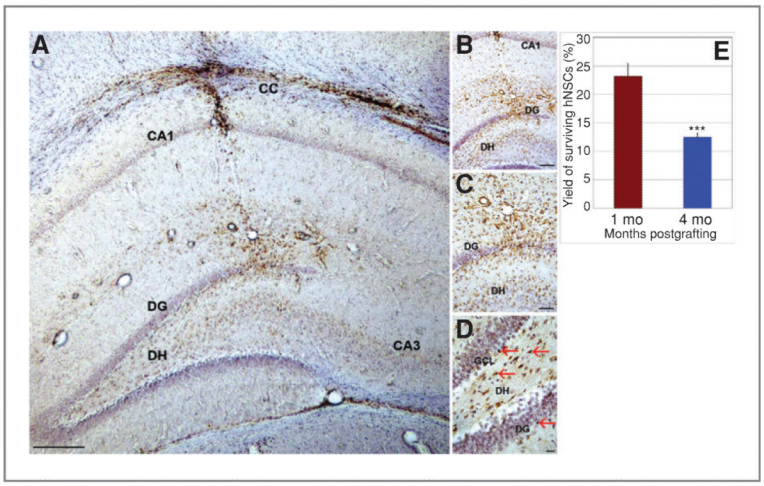

Figure 4.

Engrafted hNSCs survive and migrate in the host hippocampus. At 1 month postengraftment, hNSCs showed extensive migration from the injection site throughout the hippocampus [DG, DH, granule cell layer (GCL), CA1 and CA3 subfields, and partially in the CC; magnification ×4–40 (in A–D)]. Grafted cells were detected by BrdUrd immunostaining (dark brown nuclei, indicated by red arrows; D) and counterstained with hematoxylin. Images were derived from irradiated animals engrafted with hNSCs and analyzed at 1 month postgrafting. Enumeration of transplanted hNSCs by unbiased stereology revealed that 23% and 12% of the engrafted cells survived at 1- and 4-month postgrafting time points, respectively (E). Scale bars: A, 200 μm; B, 100 μm; C, 50 μm; D, 20 μm. ***, $P = 0.043$ comparing 1-month and 4-month postengraftment groups.

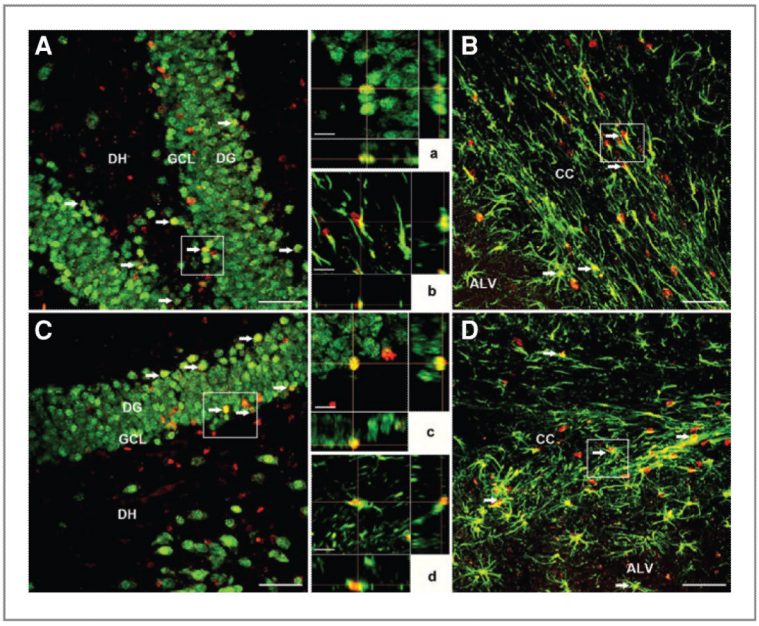

Figure 5.

Differentiation of transplanted hNSCs in the irradiated hippocampus. At 1 month postgrafting (A, B and a, b), BrdUrd-positive (red) hNSCs differentiated into NeuN-positive (green) mature neurons (A and a) and GFAP-positive (green) astrocytes(Bandb)as visualizedby dual labeling of neuron- or astrocyte-specific markers. Similar phenotypes were observed at 4 months postgrafting (C, D and c, d), where BrdUrd-positive (red) engrafted cells were colabeled with markers of mature neurons (NeuN, green; C and c), and astrocytes (GFAP, green; D and d). Arrows indicate dual labeled grafted cells, and boxes represent regions magnified for orthogonal Z-stacks (in A–D). Orthogonal reconstructions of $BrdUrd^+/NeuN^+$ colabeled cells (a and c) and $BrdUrd^+/GFAP^+$ colabeled cells (b and d) are shown at each postgrafting time point. GCL, granule cell layer; ALV, alves of hippocampus; DG, dentate gyrus; DH, dentate hilus. Scale bars: A–D, 50 μm; a–d, 10 μm.

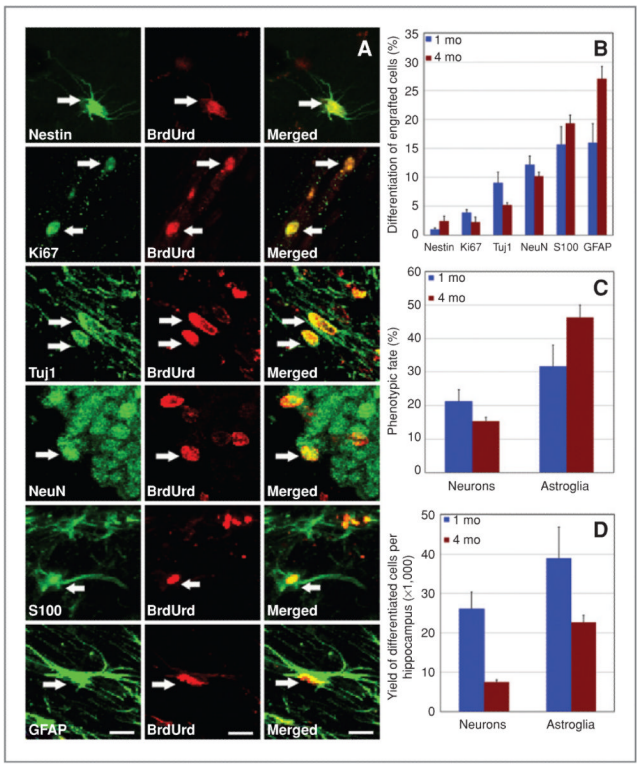

Figure 6.

Transplanted hNSCs differentiated into neuronal and astrocytic phenotypes at 1 and 4 months postengraftment. A and B, hNSCs positive for BrdUrd occasionally expressed the cell-cycle marker (Ki67) and multipotent marker (nestin). Engrafted ($BrdUrd^+$) cells differentiated into immature ($Tuj1^+$) and mature ($NeuN^+$) neurons (A and B). The majority of engrafted ($BrdUrd^+$) cells differentiated into mature ($S100^+$, S100ß protein) and immature ($GFAP^+$) astrocytes (A and B). Arrows indicate dual-labeled engrafted cells. The percentage (C) and yield (D) of differentiated hNSCs within each hemisphere of the irradiated rat brain. Scale bars: A, 5 μm.

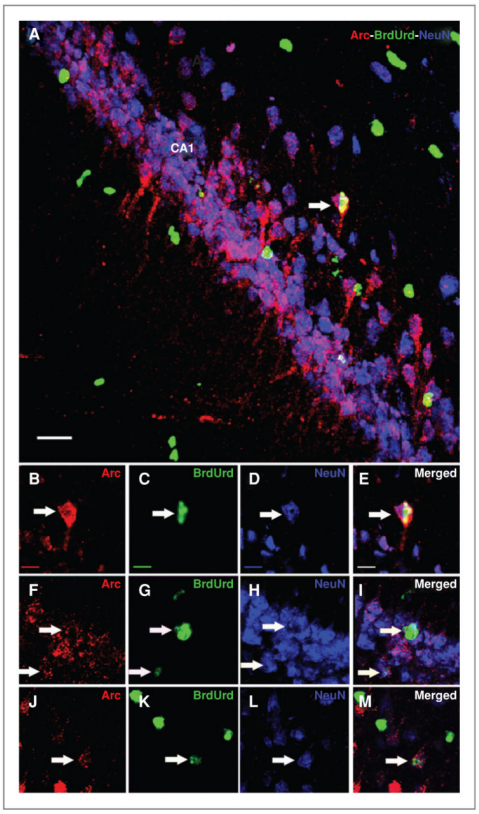

Figure 7.

HNSC graft–derived cells express behaviorally induced Arc in the irradiated hippocampus. Irradiated animals engrafted with hNSCs and subjected to a hippocampal-dependent novelty exploration task at 1 month postgrafting were rapidly processed for the isolation and analysis of brain tissues. Engrafted hNSCs (BrdUrd + cells, green; A, C, G, and K) + differentiated into NeuN-positive mature neurons (blue; A, D, H, and L) and expressed Arc (red; A, B, F, and J) as visualized by the triple labeling of neuron- and Arc-specific markers (A, E, I, and M). Arrows indicate triple-labeled cells. Scale bars: A, 50 μm; B–M, 10 μm.